Supplementary Information for:

One-pot microwave synthesis of core-shell C@Bi_2S_3 nanoflake-like structure for humidity-dependent photodetection applications

Marcin Godzierz[1,*], Sonia Gorawska[1,2], Krystian Mistewicz[3], Łukasz Otulakowski[1], Karolina Olszowska[1], Viktoriia Talaniuk[1], Anna Gawron[1], Mirosława Pawlyta[4], Urszula Szeluga[1]

1 – Centre of Polymer and Carbon Materials, Polish Academy of Sciences, Curie-Skłodowskiej 34 Str., 41-819 Zabrze, Poland

2 - Silesian University of Technology, Joint Doctoral School, Akademicka 2A, 44-100 Gliwice, Poland

3 – Silesian University of Technology, Institute of Physics – Centre for Science and Education, Krasińskiego 8, 40-019 Katowice, Poland

4 – Silesian University of Technology, Materials Research Laboratory, Faculty of Mechanical Engineering, Konarskiego 18 A, 44-100 Gliwice, Poland

Corresponding author: mgodzierz@cmpw-pan.pl

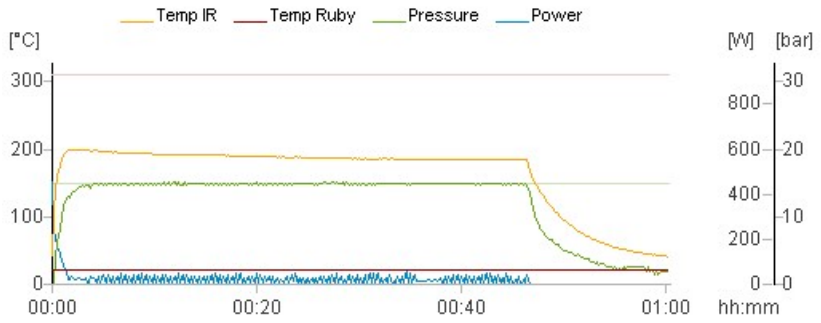

Fig. S1. Changes of pressure and temperature over synthesis of core-shell C@Bi_2S_3 nanoflakes.

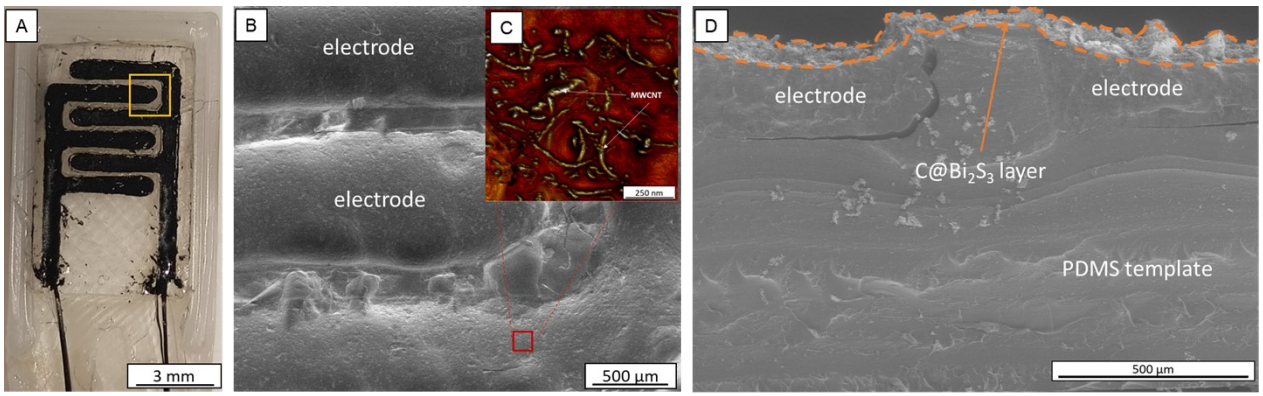

Fig. S2. The digital photograph (A) of fabricated sensor platform, SEM microphotograph (B) from square marked in digital photo, AFM image (C) from red square marked in SEM microphotograph and SEM microphotograph (D) of photodetectors' cross-section, with visible C@Bi_2S_3 layer on the top.

Table S1. Values of bandgap energy reported in the literature for bismuth sulifde.

Material	**Method of material preparation**	**Energy band gap value**, eV	**Band gap type**	**Ref.**
Bi_2S_3 film	atomic layer deposition	1.03	indirect	[1]
Bi_2S_3	not applicable	1.32	indirect	[2]
Bi_2S_3 film	physical vapor deposition	1.32 – 1.36		[3]
Bi_2S_3 film	reactive evaporation	1.38	direct	[4]
Bi_2S_3 nanoflowers	hydrothermal method	1.39	direct	[5]
Bi_2S_3 film	electrochemical synthesis	1.4	direct	[6]
Bi_2S_3 nanosheets	hydrothermal vulcanization	1.41	direct	[7]
Bi_2S_3 nanocrystals	organometallic synthesis	1.443		[8]

Bi_2S_3 nanowires	hydrothermal vulcanization	1.46	direct	[7]
Bi_2S_3 nanoribbons	hydrothermal vulcanization	1.47	direct	[7]
Bi_2S_3	not applicable	1.492	indirect	[9]
Bi_2S_3 film	atomic layer deposition	1.56	direct	[1]
Bi_2S_3 film	chemical bath deposition	1.56	direct	[10]
Bi_2S_3 film	successive ionic layer adsorption and reaction	1.61	direct	[11]
Bi_2S_3 film	pulse-plating method	1.68	direct	[12]
Bi_2S_3	microwave synthesis	1.34(2)	direct	[13]
Bi_2S_3-PVA_{high}	PVA-assisted microwave synthesis	1.41(1)	direct	
Bi_2S_3-PVA_{low}	PVA-assisted microwave synthesis	1.43(3)	direct	
μ-Bi_2S_3	PVP-assisted microwave synthesis	1.36(2)	direct	[14]
sμ-Bi_2S_3	PVP-assisted microwave synthesis	1.41(1)	direct	
C@Bi_2S_3 nanoflakes	PEG-assisted microwave synthesis	1.33(3)	direct	this work

Table S2. Values of *n* exponents of dependence $I \sim U^n$ determined for the ohmic regime ($U < U_{tr}$) and space charge limited current regime ($U > U_{tr}$) under different illumination conditions, where U_{tr} denotes a transition voltage.

	RH, %	*n exponent*
Dark condition ($I_L = 0$)	75	1.461
	55	1.379
	40	1.385
Red light illumination (λ = 629 nm, I_L = 53.4 μW/cm^2)	75	1.460
	55	1.403
	40	1.409
Blue light illumination (λ = 465 nm, I_L = 69.0 μW/cm^2)	75	1.381
	55	1.389
	40	1.369
Green light illumination (λ = 522 nm, I_L = 78.9 μW/cm^2)	75	1.379
	55	1.381
	40	1.396
White light illumination (I_L = 178.1 μW/cm^2)	75	1.364
	55	1.369
	40	1.382

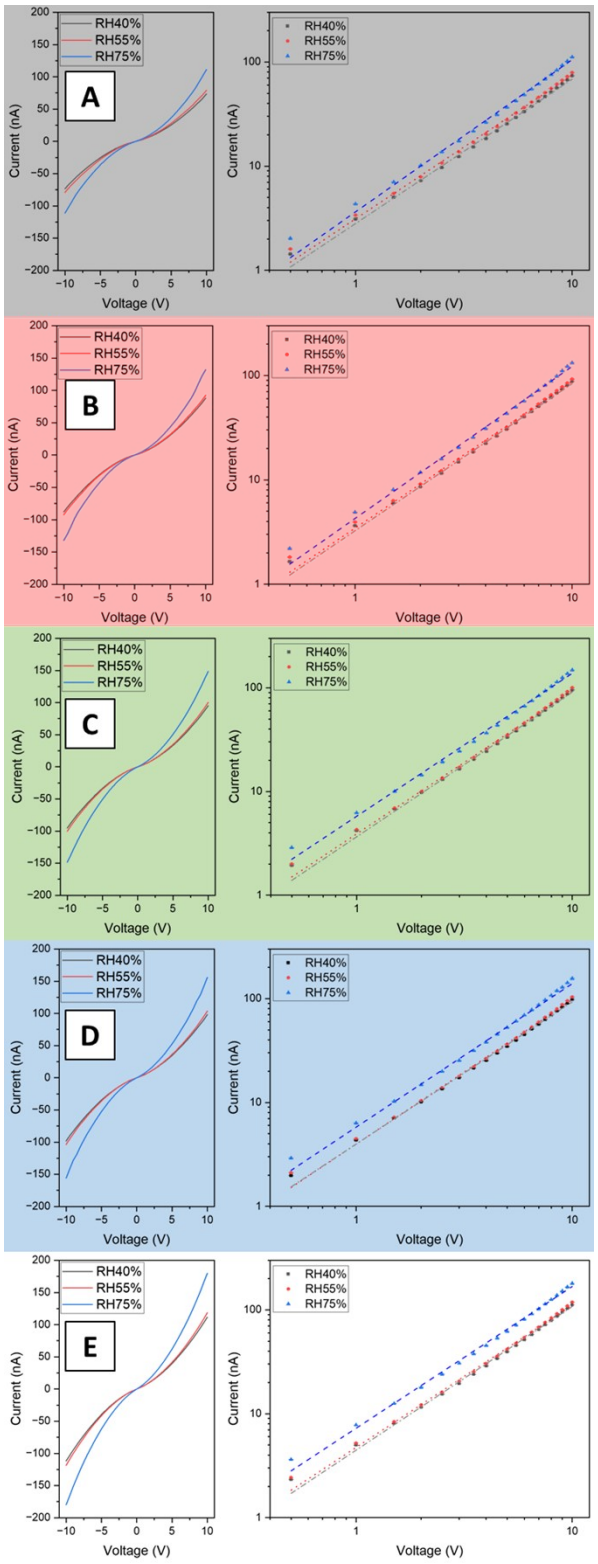

Fig. S3. Humidity-dependent current-voltage characteristics in dark (A), and under red (B, λ = 629 nm), green (C, λ = 522 nm), blue (D, λ = 465 nm) and white light (E) illumination. Right graphs show log-log plot, with two fitted curves up to 3V and above 3V (see Table S1).

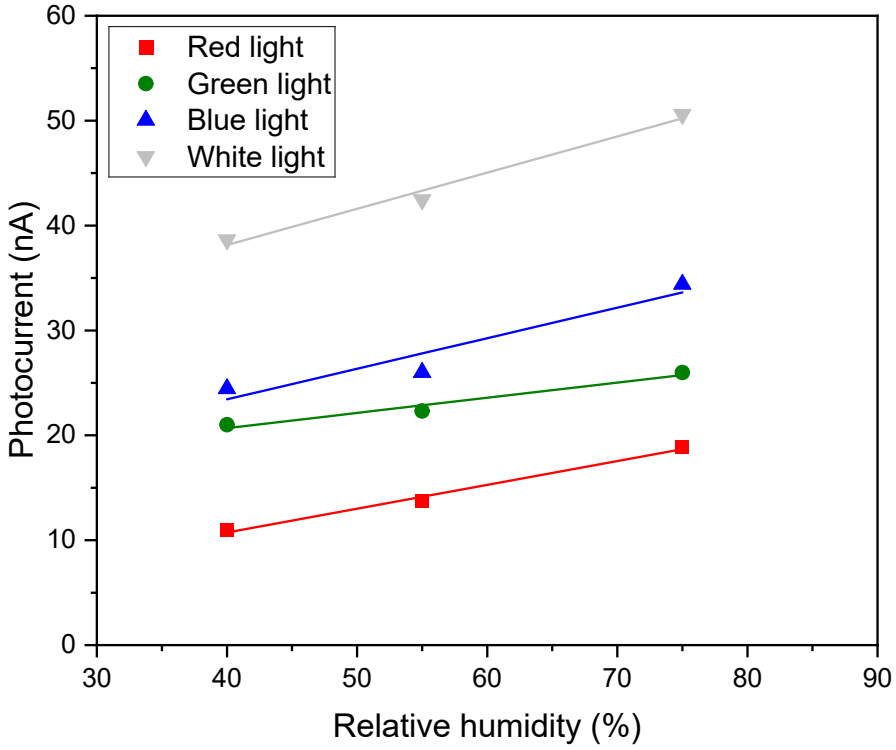

Fig. S4. The relationship between relative humidity and photocurrent induced by red light (λ = 629 nm, I_L = 53.4 μW/cm^2), green light (λ = 522 nm, I_L = 78.9 μW/cm^2), blue light (λ = 465 nm, I_L = 69.0 μW/cm^2), and white light (I_L = 178.1 μW/cm^2).

Table S3. The values of the power exponent determined by best fitting the theoretical dependence of light intensity on photocurrent (Equation (3)) to experimental data presented in Figures 8A-C.

Light color	**The power exponent *γ***		
	***RH* = 40%**	***RH* = 55%**	***RH* = 75%**
Red (λ = 629 nm**)**	0.575(7)	0.562(3)	0.484(2)
Green (λ = 522 nm**)**	0.661(1)	0.568(4)	0.547(4)
Blue (λ = 465 nm**)**	0.689(3)	0.666(6)	0.649(5)
White	0.669(2)	0.648(5)	0.611(6)

References

1 N. Mahuli, D. Saha and S. K. Sarkar, *J. Phys. Chem. C*, 2017, **121**, 8136–8144.

2 H. Koc, H. Ozisik, E. Deligöz, A. M. Mamedov and E. Ozbay, *J. Mol. Model.*, 2014, **20**, 2180.

3 S. ten Haaf, H. Sträter, R. Brüggemann, G. H. Bauer, C. Felser and G. Jakob, *Thin Solid Films*, 2013, **535**, 394–397.

4 J. Lukose and B. Pradeep, *Solid State Commun.*, 1991, **78**, 535–538.

5 S. Sharma and N. Khare, *Colloid Polym. Sci.*, 2018, **296**, 1479–1489.

6 Z. Grubač, J. Katić and M. Metikoš-Huković, *J. Electrochem. Soc.*, 2019, **166**, H433.

7 Y.-C. Liang and T.-H. Li, 2022, **11**, 284–297.

8 M. Aresti, M. Saba, R. Piras, D. Marongiu, G. Mula, F. Quochi, A. Mura, C. Cannas, M. Mureddu, A. Ardu, G. Ennas, V. Calzia, A. Mattoni, A. Musinu and G. Bongiovanni, *Adv. Funct. Mater.*, 2014, **24**, 3341–3350.

9 H. Ben Abdallah and W. Ouerghui, *Opt. Quantum Electron.*, 2021, **54**, 20.

10 H. Moreno-García, S. Messina, M. Calixto-Rodriguez and H. Martínez, *Appl. Surf. Sci.*, 2014, **311**, 729–733.

11 M. Suresh Kumar, S. P. Madhusudanan, K. Mohanta and S. K. Batabyal, *Mater. Res. Express*, 2020, **7**, 15909.

12 F. Ding, Q. Wang, S. Zhou, G. Zhao, Y. Ye and R. Ghomashchi, *R. Soc. Open Sci.*, 2020, **7**, 200479.

13 K. Mistewicz, M. Godzierz, A. Gawron, Ł. Otulakowski, A. Hercog, K. Kurtyka, S. Hajra and H. J. Kim, *J. Mater. Chem. C*, 2024, **12**, 15691–15703.

14 M. Godzierz, K. Mistewicz, A. Gawron, K. Kurtyka, Ł. Otulakowski and T. Kanti Das, *J. Alloys Compd.*, , DOI:10.1016/j.jallcom.2024.176820.